Spatial and temporal variability of SST and ocean color in the Gulf of Maine based on cloud-free SST and chlorophyll reconstructions in 2003–2012

Yizhen Li *, Ruoying He

Department of Marine, Earth, and Atmospheric Sciences, North Carolina State University, Raleigh, NC 27695, United States

ARTICLE INFO

ABSTRACT

The spatial and temporal variability of sea surface temperature (SST) and Chlorophyll-a (Chl-a) in the Gulf of Maine (GOM) is examined using daily, cloud-free Data INterpolating Empirical Orthogonal Function (DINEOF) reconstructions during 2003–2012. The utility of the DINEOF SST and Chl-a is demonstrated through direct comparisons with buoy- and ship-based observations. EOF analyses of cloud-free products are further used to quantify the SST and Chl-a variability on seasonal to inter-annual timescales. The first mode of SST is dominated by an annual cycle in response to net surface heat flux, with SST lagging surface flux by ~57 days. The second mode of SST underscores interactions between GOM, the Scotian Shelf, and the slope sea in response to the basin scale atmospheric forcing represented by the North Atlantic Oscillation. The third mode correlates well with the evolution of Scotian Shelf-slope frontal displacement. The first EOF mode of Chl-a is dominated by a winter–spring bloom and a fall bloom, with a spatial distribution modified by the tidal mixing that facilitates nutrient delivery from the deep ocean. The second EOF mode is likely associated with a winter bloom in the warm slope sea, where the low-frequency variations of second modes of SST and Chl-a are in phase, suggesting a possible coupling between physical and biological responses to atmospheric forcing. The third mode of the Chl-a is likely associated with freshening events associated with advection of the Scotian Shelf Water, which enhance stratifications in the eastern GOM.

Published by Elsevier Inc.

1. Introduction

The Gulf of Maine (GOM) is a semi-closed marginal sea off the U.S. northeast coast (Fig. 1). Extensive research in the past on regional circulation and hydrography have studied processes on synoptic (e.g., Churchill, Pettigrew, & Signell, 2005; He et al., 2005), seasonal (e.g., Lynch, Ip, Naimie, & Werner, 1996; Xue, Chai, & Pettigrew, 2000), and inter-annual time scales (e.g., Li, He, & McGillicuddy, in press; Pettigrew et al., 2005, 1998). The mean gulf circulation is cyclonic (Bigelow, 1927), and modulated by both local and remote forcing. Local forcing includes strong tidal mixing and rectifications (e.g., Garrett, 1972; Limeburner & Beardsley, 1996; Lynch, Holboke, & Maimie, 1997), surface heat flux (e.g., Xue et al., 2000) and wind (e.g., He & McGillicuddy, 2008). Remote influence stems from surface inflow of relatively cold, fresh Scotian Shelf (SS) water through Cape Sable (Smith, 1983), intrusions of Labrador subarctic Slope Water (LSW) and the Atlantic Warm Slope Water (WSW) through the Northeast Channel (NEC). From time to time, Gulf Stream eddies can also play a role in shaping the slope sea circulation, which in turn affects circulation

and transport in the GOM (e.g., Bisagni & Smith, 1998; Chaudhuri, Gangopadhyay, & Bisagni, 2009).

The GOM is known for high biological productivity. Significant seasonal phytoplankton blooms occur every fall and spring, although the exact timings vary region by region in the gulf due to differences in hydrodynamics, bathymetry, stratification, mixing processes, and nutrient uptake (e.g., O'Reilly & Busch, 1984; O'Reilly, Evans-Zetlin, & Busch, 1987; Yoder, Schollaert, & O'Reilly, 2002; Thomas, Townsend, & Weatherbee, 2003). Research to date on plankton bloom and Chl-a variations have relied largely on episodic ship survey data or time series observations measured by buoys. An inherent practical limitation of this approach is data gaps spatially (Herman et al., 1991; Holligan, Balch, & Yentsch, 1984; O'Reilly et al., 1987; Townsend, Cammen, Holligan, Campbell, & Pettigrew, 1994; Townsend & Thomas, 2001; Townsend & Thomas, 2002). Satellite remote sensing provides a useful means to routinely sample the surface ocean over a larger spatial context. Early studies using remote sensing have addressed the relationship between SST front and shelfbreak bloom (e.g., Ryan, Yoder, & Cornillon, 1999), ocean environmental variability and its linkage with shellfish toxicity (e.g., Luerssen, Thomas, & Hurst, 2005; Thomas, Weatherbee, Xue, & Liu, 2010), coastal circulation in eastern and western GOM (e.g., Pettigrew et al., 2005), and mesoscale eddy activities (e.g., Churchill et al., 2005). Various forms of remote sensing data including instantaneous snapshots (Yoder, O'Reilly, Barnard, Moore, &

* Corresponding author. Tel.: +1 919 513 0943.
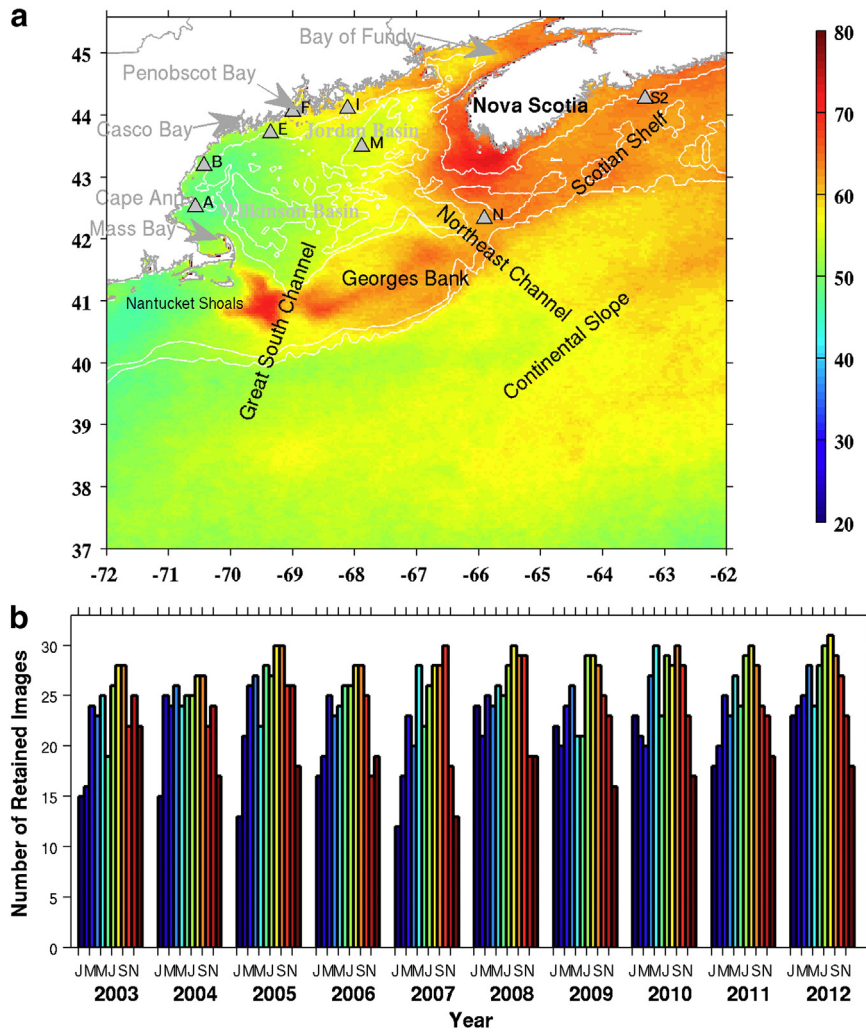 E-mail address: yli15@ncsu.edu (Y. Li).

Fig. 1. (a) Spatial distribution of the percent of cloud coverage in MODIS SST during 2003–2012. Major geographic locations and 100- and 200-m isobaths in the Gulf of Maine are shown. Also shown are the locations for NERACOOS buoys A, B, E, F, I, M, and N. Surface temperature data measured by these buoys are used to compare with satellite measured SST. Chl-a concentrations measured by buoy Station 2 (S2) on the Scotian Shelf are used to compare with their satellite counterparts. (b) Number of retained daily images used for the reconstruction of SST in each month during 2003–2012. Only images with less than 98% cloud coverage are retained for the reconstruction.

Ruhsam, 2001), monthly composite (e.g., Thomas et al., 2003), and long-term climatology (Ji et al., 2007; Yoder et al., 2002) were used/derived to study temporal and spatial variation of phytoplankton and Chl-a in the GOM, as well as frontal displacement (Ullman & Cornillon, 1999). While satellites provide more routine and consistent temporal sampling, their data can be quite gappy due to cloud cover problem (e.g., Miles & He, 2010). As a result, compromises have to be made by computing composite averages over different time periods (e.g., weekly or monthly), limiting the ability of remote sensing observation in resolving synoptic processes. In addition, previous SST and Chl-a studies for the GOM covered a short span of time in the 1990s and early 2000s (Thomas et al., 2003) or focused on seasonal climatology (Yoder et al., 2002). As such, a study of seasonal and interannual variability based on cloud-free SST and ocean color data for the GOM based on novel reconstruction techniques in recent decade is therefore highly needed.

To do this, we used concurrent sea surface temperature (SST) and ocean color observations obtained by MODIS (Moderate Resolution Imaging Spectroradiometer) to investigate simultaneous variations in SST and surface Chl-a. The MODIS sensor was launched in May, 2002 aboard the synchronous polar orbiting satellite Aqua, thus can provide useful information for surface thermal and productivity structures during the past decade. MODIS is only capable of viewing in the visible and infrared

wave bands, thus almost all images have cloud cover to various extents. Taking GOM for instance, we see that the average percent of cloud coverage is over 60% of the total spatial coverage, with over 80% cloud cover over the Georges Bank and Scotian Shelf (Fig. 1a). To overcome t cloud-cover problem in the satellite data, we utilized a new daily, high-resolution, cloud-free SST and Chl-a analysis for the GOM using the Data INterpolating Empirical Orthogonal Function (DINEOF) (Alvera-Azcárate, Barth, Beckers, & Weisberg, 2007; Alvera-Azcárate, Barth, Sirjacobs, & Beckers, 2009). Similar approach has been successfully applied to study ocean color and SST variability in the South Atlantic Bight (Miles, He, & Li, 2009), the North Sea (Sirjacobs et al., 2011) and Mediterranean Sea (Volpe, Buongiorno Nardelli, Cipollini, Santoleri, & Robinson, 2012). This new analysis technique provides an accurate space and time reconstruction of otherwise cloud-covered SST and Chl-a fields, allowing us to study SST and Chl-a co-variability in the GOM and its adjacent seas, and furthermore, explore their relations with surface forcing and basin-scale deep ocean forcing.

We start in Section 2 with an introduction of satellite data, in-situ observations, atmospheric forcing, and climate indices used in the study, followed by a brief description of DINEOF method we used for cloud-free SST and Chl-a reconstructions. Section 3 presents the comparison of our analysis against buoy- and ship-based observations, and

mean distributions of SST and Chl-a. Further statistical analyses of their variability and possible driving mechanisms are discussed in Section 4, followed by summary and conclusion in Section 5.

2. Data and methods

The concurrent, daily 4-micon daytime MODIS SST and Chl-a data in January 2003–December 2012 were used in this study. Both SST and Chl-a data used in this study were level 3 fields provided by NASA Goddard Space Flight Center (GSFC, http://modis.gsfc.nasa.gov/). The level 3 product were collected in a 4-km spatial resolution from 37°N–46°N in latitude and 72°W–62°W in longitude. The snapshots with over 98% cloud coverage for both SST and Chl-a were removed to ensure accurate reconstruction (Alvera-Azcárate et al., 2009). Fig. 1b shows the number of images retained for each month during 2003–2012. The available images range from 12 to 20 days in winter months to over 20 days in summer months. Of the initial 3653 days, 2872 daily snapshots were retained for reconstruction.

In addition to satellite images, ancillary data used including ocean temperature (1-m below the surface) measured by buoys of Northeast Regional Association of Coastal and Ocean Observing Systems (NERACOOS). Buoys A, B, and E are in the western GOM, buoys F and I are near the Penobscot Bay river mouth, and in the eastern GOM respectively, buoys M and N are in the Jordan Basin, and in the Northeast Channel, respectively (Fig. 1a). In addition, in-situ surface Chl-a observations from the Atlantic Zone Monitoring program (AZMP) and GOM Chl-a climatology (Rebuck, 2011) were used to compare with our reconstructed Chl-a. Daily and winter-only (DJFM) North Atlantic Oscillation (NAO) index and Scotian Shelf-slope front climatological indices derived by AZMP program were also utilized to quantify the variability of SST and its possible linkage with large scale forcing. We also computed the net heat flux from the NOAA NCEP to quantify the impact of surface forcing on SST variability.

Daily, cloud-free SST and Chl-a reconstructions were performed using the Data INterpolation Empirical Orthogonal Function (DINEOF) method. This approach identifies dominant spatial and temporal patterns and fills in missing points accordingly (Alvera-Azcárate, Barth, Rixen, & Beckers, 2005; Alvera-Azcárate et al., 2007; Miles & He, 2010; Miles et al., 2009). While obtaining similar or better reconstruction of surface satellite data, it is found to be about 30 times faster than tradition OI method (e.g., He, Weisberg, Zhang, Muller-Karger, & Helber, 2003; Miles et al., 2009; Beckers, Barth, & Alvera-Azcarate, 2006). No a priori information (such as decorrelation scale) is required and can use different types of observations (e.g., SST and Chl-a) to perform multivariate reconstruction. To decrease the spurious temporal variations in the temporal EOFs, a filtering of the temporal covariance matrix was applied to obtain more realistic reconstructions (Alvera-Azcárate et al., 2009).

We present here a concise description of the DINEOF procedure and details of parameters as follows. First, the initial data input (X) is obtained by subtracting the temporal mean and setting the missing data to zero. Second, a Singular Value Decomposition (SVD) of X is performed, which fills in missing data with the best guess by the equation: $X_{i,j} = \sum_{p=1}^{k} \rho_p (u_p)_i (v_p^T)_j$, where i and j in X are the temporal and spatial indices respectively. K is the number of the EOF modes, u_p and v_p are the P_{th} column of the spatial and temporal functions of EOF, and ρ_p (where p = 1, 2,...,k) represents the corresponding singular values. The value of k is set as 50 in this study. In step 2, repeat iteratively k times or until convergence, using the previous best guess as the initial value for the subsequent iteration, where convergence is defined by a present Laczos convergence threshold (10^{-8} in this study) of the absolute value of the difference between the SVD of the current and the previous iterations. Third, a cross-validation technique is applied to decide the optimal number of EOF retains for the final reconstruction. In the final step, the first and second steps are repeated using only the optimal

number of EOF modes and the temporal mean is subsequently added back to the reconstructed matrix to obtain the interpolated dataset.

Similar as Alvera-Azcárate et al. (2007) and Miles et al. (2009), we utilized a multivariate adaptation of DINEOF for the reconstruction. The concurrent SST, Chl-a and one-day lagged SST to reconstruct SST fields, and use concurrent Chl-a, SST and one-day lagged Chl-a to reconstruct Chl-a fields. A natural logarithmic scale transformation was applied to Chl-a field before the reconstruction, the same approach used in Miles et al. (2009). We chose 1-day as the lag time because we found that it produced the best reconstruction results. We chose to construct fields at every spatial point in the domain to avoid cold spikes at cloud edges and other sources of noise in the initial matrix (Alvera-Azcárate et al., 2007). The resulting 10-year reconstructed SST and Chl-a are available online at: http://omgrhe.meas.ncsu.edu/Group/.

In Section 4, to better discern the spatial heterogeneity, the degree of coherence and temporal evolution of SST and Chl-a fields, a traditional empirical orthogonal function (EOF) analysis was further applied to the daily, cloud-free DINEOF SST and Chl-a datasets. Each data is organized in an $M \times N$ matrix, where M and N represent the spatial and temporal elements respectively. Taking SST for instance, the matrix $T(x,t)$ can be represented by $T(x,t) = \sum_{n=1}^{N} an(t)Fn(x)$, where $an(t)$ are the temporal evolution functions and $F_n(x,y)$ the spatial eigen-functions for each EOF mode respectively. Prior to EOF analysis, the temporal means are removed from the original data using: $T'(x,t) = T(x,t) - \frac{1}{N} \sum_{j=1}^{N} T(x,t_j)$, where $T'(x,t)$ are the resulting residuals (anomalies). The first three modes are decomposed to analyze the major variability in SST and Chl-a and linkage to local and basin-scale forcing.

3. Results

3.1. Validations of the reconstructed DINEOF SST and Chl-a

The ability of the DINEOF to reconstruct cloud-covered SST and Chl-a is demonstrated in Fig. 2 as an example. The raw SST only covered a part of Bay of Fundy, Georges Bank and a portion of slope region on February 07, 2011, and conditions in the western GOM, Scotian Shelf, and part of slope area was invisible due to cloud cover (Fig. 2a). The cloud-free DINEOF SST (Fig. 2b) presented a complete structure of SST. There was relatively smoother transition between warm slope water to colder GOM. The colder SST in the Scotian Shelf is also clearly visible. The concurrent gappy Chl-a (Fig. 2c) presented limited information except for Georges Bank, Scotian Shelf and a small patchiness in Nantucket Island. The cloud-free Chl-a (Fig. 2d) construction indicated lowest Chl-a concentration in the continental slope south of Georges Bank, where warm slope water was present. Higher Chl-a concentration (2 mg/m^{-3}) was present in the northern flank of George Bank. A strong bloom permeated the Bay of Fundy and Cape Cod and adjacent area. Consistent with earlier finding identified for mesoscale variability in the Middle Atlantic Bight shelfbreak (He, Chen, Moore, & Li, 2010) and in the Gulf of Mexico (Zhao and He (2012), the Chl-a concentration in the warm slope sea and shelfbreak area was spatially negatively correlated with SST.

The DINEOF cloud-free, daily SST was validated against daily-mean 1-m ocean temperature measured by seven NERACOOS buoys (Table 1). With seasonal cycle retained, the correlation coefficients are higher than 0.96 at all seven buoys. Both raw SST and DINEOF reconstructed SST well align with observations (not shown), suggesting that DINEOF reconstruction is a good representation of reality. With seasonal removed, the coefficients are also statistically significant with correlation ranging from 0.53 to 0.73. Root mean square difference between DINEOF SST and observations are less than 2 °C at all buoys. Given the uncertainty of MODIS data retrievals, the spatial aliasing between the 4-km DINEOF footprint and actual buoy locations, and the mismatch between surface skin temperature measured by satellite and 1-m bulk
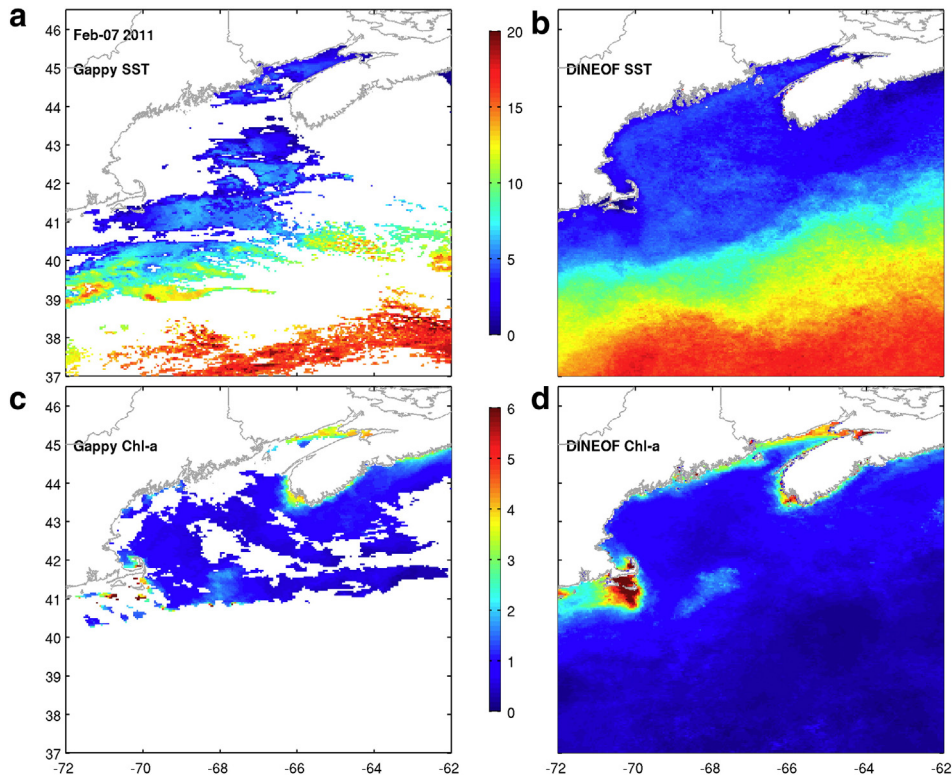
Fig. 2. The (a) cloud-covered and (b) DINEOF reconstructed SST (°C); and (c) gappy and (d) DINEOF reconstructed Chl-a concentrations (mg m^{-3}) on February 07, 2011.

temperature measured by buoys, we conclude that the DINEOF is statistically a robust representation of realistic SST variations.

We also compared DINEOF Chl-a reconstruction with limited in-situ Chl-a observations. To do that, we averaged the DINEOF cloud-free Chl-a

into monthly-mean and compared with monthly Chl-a climatology based on in-situ observations (Rebuck, 2011). The DINEOF Chl-a produces the seasonal evolution of the bloom in the GOM interior reasonably well, presenting a spring bloom in April–May and a weaker bloom from October to November. There is an overall correlation coefficient of 0.6 between DINEOF and observed Chl-a, although the reconstructed Chl-a overestimate the variability by about 50%, with a standard deviation of 1.6 and a root-mean-square difference ratio of 1.3 (not shown). Furthermore, the point comparison between DINEOF Chl-a and limited in-situ time series of scattered surface Chl-a at Station 2 (see its location in Fig. 1) is statistically significant (Fig. 3), with correlation of 0.48 based on limited observations span from 2003 to 2006. The satellite Chl-a observations is influenced by color dissolved organic matter (CDOM) and other Inherent Optical Property (IOP). In addition, uncertainty for in situ observations may stem from flurometric and/or high performance liquid chromatography (HPLC) analysis used to determine the concentration. Previous study shows that Chl-a pigment estimates based on different techniques can vary by up to 68% (Trees, Kennicutt, & Brooks, 1985).

Table 1
Buoy-observed surface temperature in comparison with the corresponding DINEOF reconstructed SST at buoys A, B, E, F, I, M and N, respectively. The buoy observations are averaged to an hourly time interval to be consistent with satellite observations.

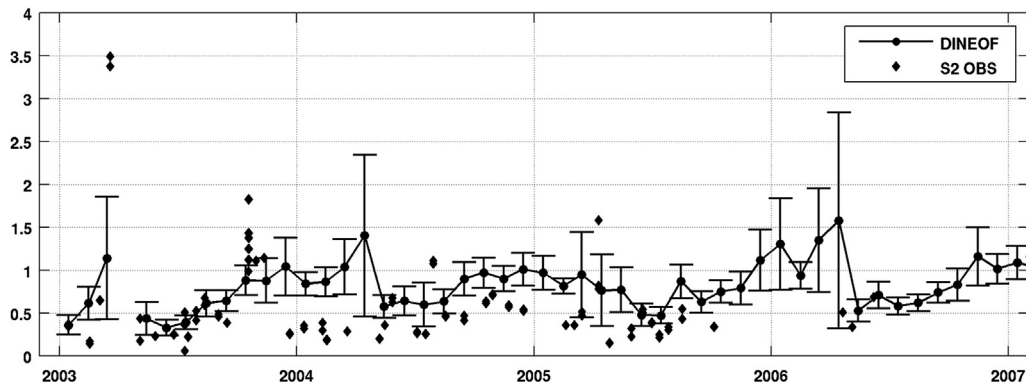| Buoy ID	Number of observations (days)	Root mean square error	Correlation coefficient (seasonal cycle retained/retained)
A	2719	1.52	0.98/0.68
B	2761	1.51	0.97/0.69
E	2845	1.43	0.97/0.73
F	2550	1.90	0.96/0.53
I	2842	1.19	0.96/0.64
M	2719	1.80	0.97/0.70
N	2379	1.65	0.96/0.64

Fig. 3. Comparison between observed Chl-a (circular dots, mg m^{-3}) at Station 2 (S2) on the Scotian Shelf and DINEOF reconstructed Chl-a (diamonds). The DINEOF Chl-a is shown in the monthly mean with error bar superimposed. Correlation coefficient between two time series is 0.48.

3.2. Monthly Climatology of SST and Chl-a

The reconstructed decade-long daily SST and Chl-a were temporally averaged to produce their respective monthly climatology for the region (Figs. 4 and 5). The SST shows a sinusoidal seasonal cycle, with persistent seasonal warming trend from winter (March) to summer (August). There is a clear temperature contrast between the gulf water and the open ocean water in spring and fall. The thermal difference reaches as high as ~4 °C between GOM and Slope Sea in August. The thermal front near the shelfbreak is however more visible in winter and spring months. Spatially, the Georges Bank, SS and eastern GOM have lower temperature compared to the western GOM, which is in part a result of stronger tidal mixing and coast water advection from Scotian Shelf (Fig. 4).

Using a four-year SeaWiFs Chl-a data, Thomas et al. (2003) derived a seasonal cycle. Here we intend to quantify the annual cycle of Chl-a as well but using a decadal-long time series. The climatological seasonal cycle of Chl-a (Fig. 5) shows larger spatial heterogeneity compared to SST. Overall, the Chl-a concentration is larger either in the coastal western GOM or in the regions with stronger tidal signals, such as northern flank of Georges Bank and Bay of Fundy. Our results show similar seasonal features identified by Thomas et al. (2003). For example, 1) there are elevated Chl-a concentrations in nearshore waters and Georges Bank in spring and fall bloom seasons. 2) The bloom in the deep basin of GOM generally follows a canonical North Atlantic bloom seasonal cycle. There is low Ch-abloom in winter, an annual maximum in March–April, decreased concentration in summer, followed by a fall
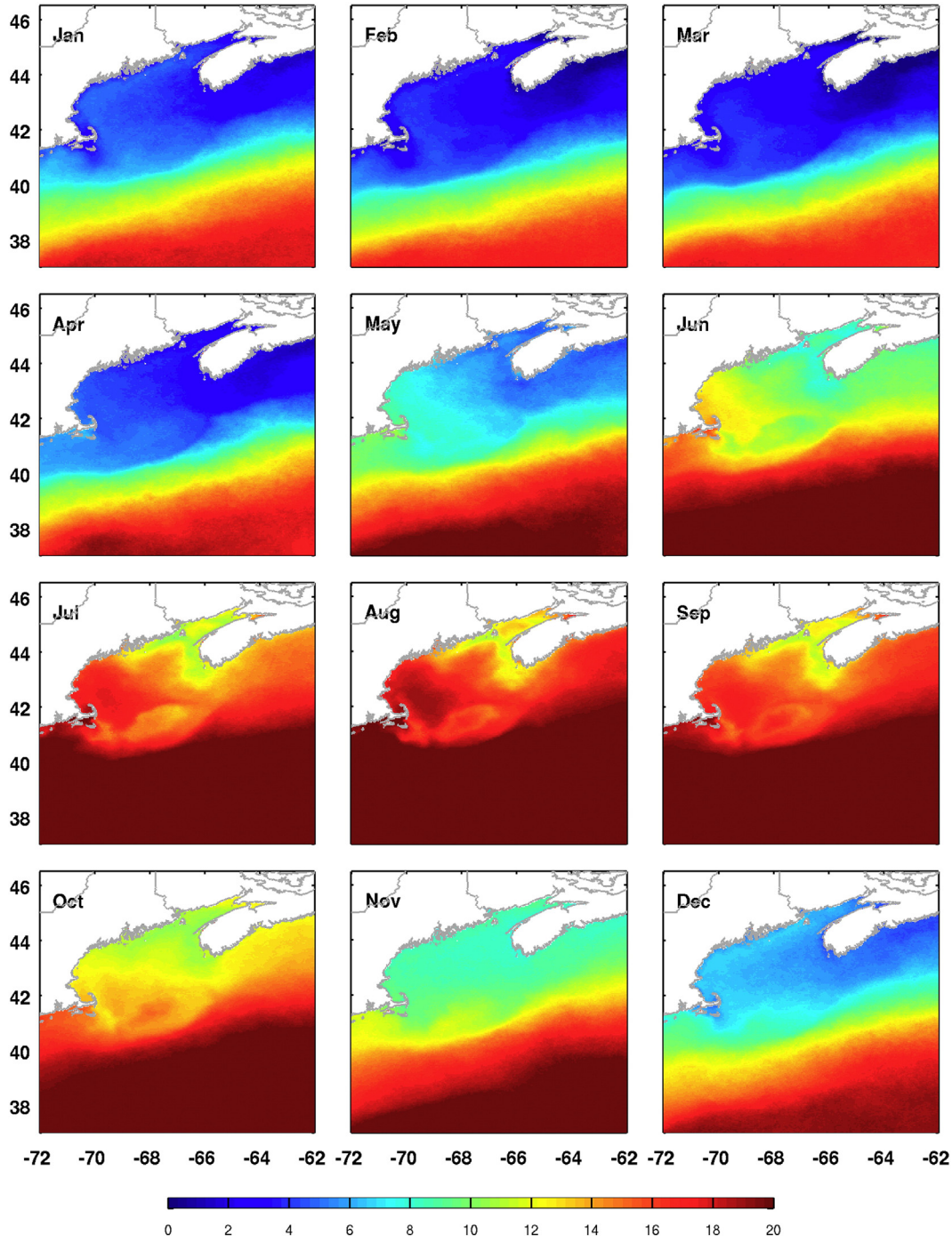

Fig. 4. Long-term SST (°C) monthly mean climatology computed from daily DINEOF SST reconstruction during 2003–2012.
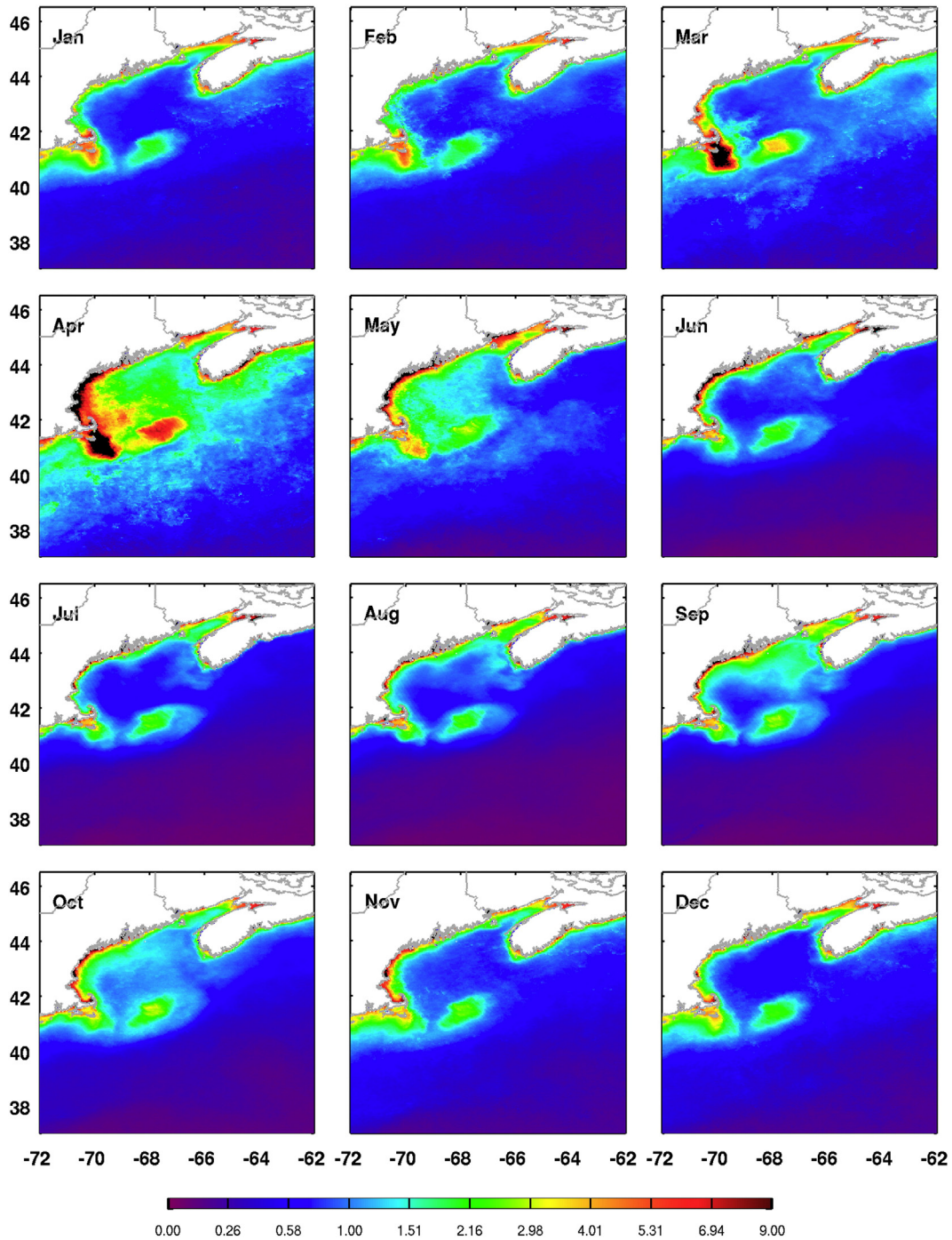
Fig. 5. Long-term Chl-a (mg m^{-3}) monthly mean climatology computed from daily DINEOF Chl-a reconstruction during 2003–2012.

bloom occurring as early as September in Jordan Basin and October–November in other regions. While the result presented herein is very much consistent with previous study, we also notice some differences in the annual seasonal cycle. Our analysis shows that the spring bloom in the SS occurs in March, which is earlier than the basin interior, whereas Thomas et al. (2003) showed almost simultaneous spring bloom in the deep basins and SS. The retreat of the spring bloom in the SS is also earlier (May) than that of the GOM gulf-wide bloom (June); Wilkinson Basin is lack of strong fall bloom compared to coastal shallow water and other deep basins in the GOM, whereas Thomas et al. (2003) showed a fall bloom in the Wilkinson Basin comparable to the coastal GOM. We speculate that these minor differences are likely

caused by the utility of different dataset (MODIS vs. SeaWiFs) and different time spans of data used in creating the climatology.

4. Discussions

4.1. Characterizing the mean spatial and temporal patterns of SST and Chl-a

The long-term mean SST (Fig. 6a) shows a smooth transition from warmer water in the slope sea to colder water near the coast. The gulf-wide averaged time series of SST is dominated by a sinusoidal seasonal cycle (blue line in Fig. 6b), superimposed by synoptic and interannual variability signals (Fig. 6c). The 60-day running mean (red line in
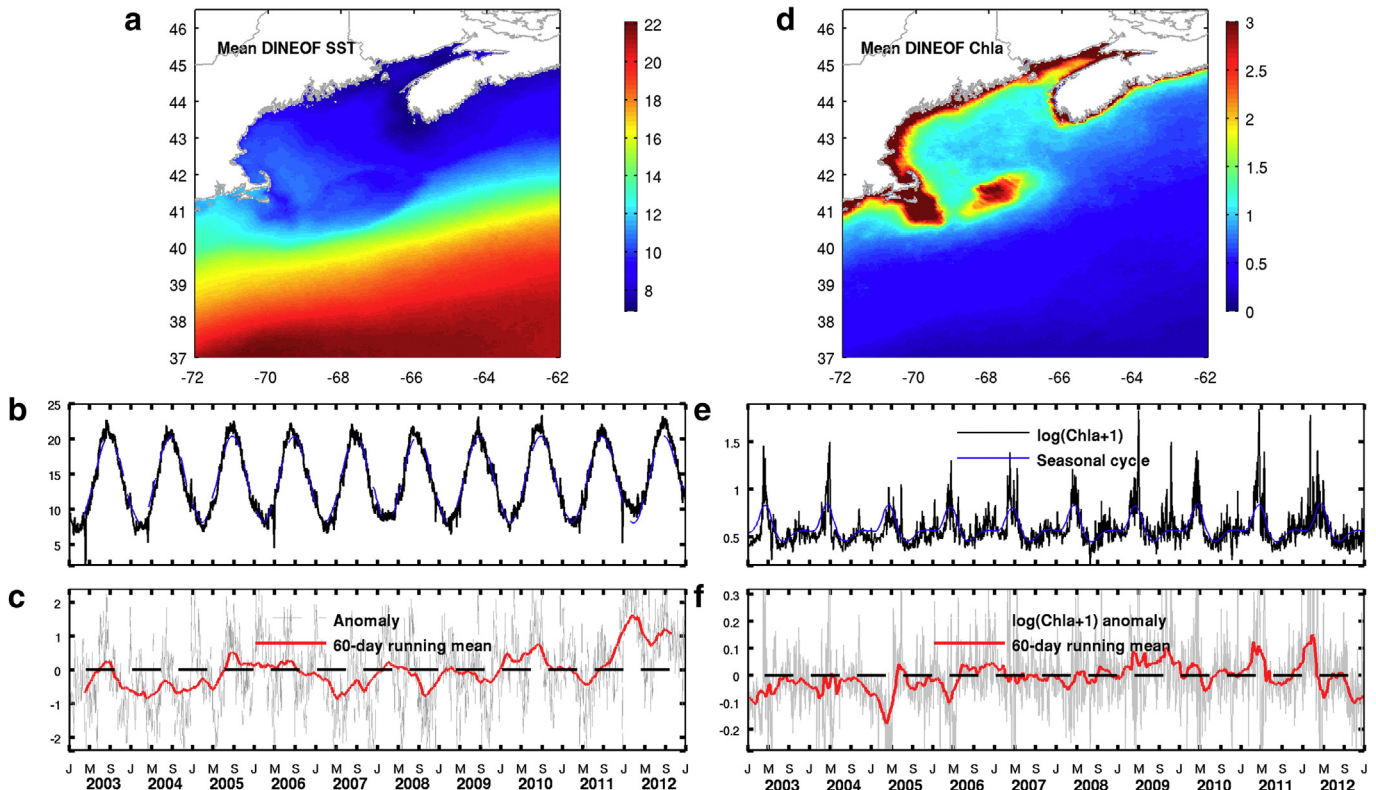
Fig. 6. (a) Long-term temporal mean of DINEOF SST (°C). (b) time series of domain-wide spatial mean SST during 2003–2012 (black line) and the seasonal cycle (blue line) associated with it. The seasonal cycle was derived by long-term averaging the daily snapshots during 2003–2012 that are on the same day of year, a similar approach as harmonic fitting but reserves secondary peaks such as the Chl-a fall bloom. (c) Time series of domain-wide spatial mean SST anomalies (in gray) and its 60-day running mean (in red); (d) long-term temporal-mean of DINEOF Chl-a concentration (mg m^{-3}); (e) time series of domain-wide spatial mean Chl-a concentration (black line) and its corresponding seasonal cycle (blue line); (f) Spatial-averaged Chl-a anomalies with seasonal cycle subtracted (in gray) and its 60-day running mean (in red); for both panels e and f, a natural logarithmic scale is applied to time series of Chl-a concentration to offer better visualizations. (For interpretation of the references to color in this figure legend, the reader is referred to the web version of this article.)

Fig. 6c) clearly shows warm SST anomalies in summer 2005 (~0.5 °C) and spring and summer 2010 (~0.7 °C). Previous studies showed that the anomalously warm temperature in summer 2005 is a consequence of increased surface net heat flux (He & McGillicuddy, 2008), and the warmer temperature in 2010 is coincident with the entrainment of warmer slope water through Northeast Channel (Li et al., in press; McGillicuddy et al., 2011). Moreover, we also noticed a positive SST anomaly (over 1 °C) throughout late 2011 and spring to summer 2012. The causes of which will be discussed in Section 4.2.

The long-term Chl-a (Fig. 6d) shows sharp decrease in Chl-a from the coastal water within the 100-m isobath to the offshore region, suggesting an inverse relationship between general pattern of Chl-a and bathymetry (O'Reilly et al., 1987). In several areas, strong tidal mixing makes more deep-ocean nutrient available for phytoplankton utilization. The spatially-averaged time series (Fig. 6f) shows clear interannual variability superimposed on the seasonal spring (April) and fall (August) blooms (Fig. 6e). A noticeable scenario is the increasing trend in the gulf-wide Chl-a from 2003–2011, which requires more subsurface nutrient observations to further investigate the underlying mechanisms.

4.2. Modes of the variability in SST and Chl-a

4.2.1. SST variability

To better discern the spatial heterogeneity, the degree of coherence and temporal evolution of temperature and Chl-a fields, an empirical orthogonal function (EOF) analysis was further applied to the daily, cloud-free DINEOF SST and Chl-a datasets. Details of the EOF are summarized in Section 2. The EOF analysis then provides spatial and temporal functions derived from the anomaly field covariances relative to the spatial mean fields (as shown in Fig. 6a and d).

The first 3 EOF modes of SST are shown in Fig. 7. The first SST EOF mode accounts for the 92.43% of the total variance. Its temporal evolution is overall dominated by an annual periodicity peaking in summer and winter, as well as the interannual variability signal such as elevated temperature anomalies in 2005, 2010, and 2012 (Fig. 7b). The spatial variation shows that SST has different phase in different region. As a result of tidal rectification, the spatial EOF is highly coincident with M-2 tidal amplitude distribution in the region. The magnitude of EOF1 is overall larger in the western GOM, SS, Nantucket Islands and southern flank of Georges Bank, and smaller in the eastern GOM, Bay of Fundy and Georges Bank where tidal mixing is high. In addition, temperature in the shallow water presents a larger variability compared to that in the slope region. This is because the variation of SST, in the first order one-dimensional sense, is inverse proportional to the water depth (e.g., He & Weisberg, 2003). As such, coastal ocean waters overall have larger seasonal cycle. In contrast, temperature in the slope region stays fairly consistent due to both increase in water depth (heat content) and persistent warm water supply from the slope sea.

The second EOF mode (accounting for 1.24% of total variance) presents combined signals including synoptic time-scale oscillations, a weak annual cycle, as well as interannual variability. PC2 reaches its peak in May–July and its minimum December to February. The exact timing of the peak varies in different years. A dipole-like feature with north–south orientation is present in the second EOF suggesting an out-of-phase variability between the slope sea and the GOM. We also note that there is a positive peak in 2008 and obvious negative peaks in summer 2010 and 2012. Thus, mode 2 is indeed an augmentation of the interannual variability signal in mode 1 for the GOM and SS. In contrast, mode 2 provides a positive (negative) temperature anomaly in 2008 (2010/2012), which is offsetting with the SST interannual variations in mode 1.
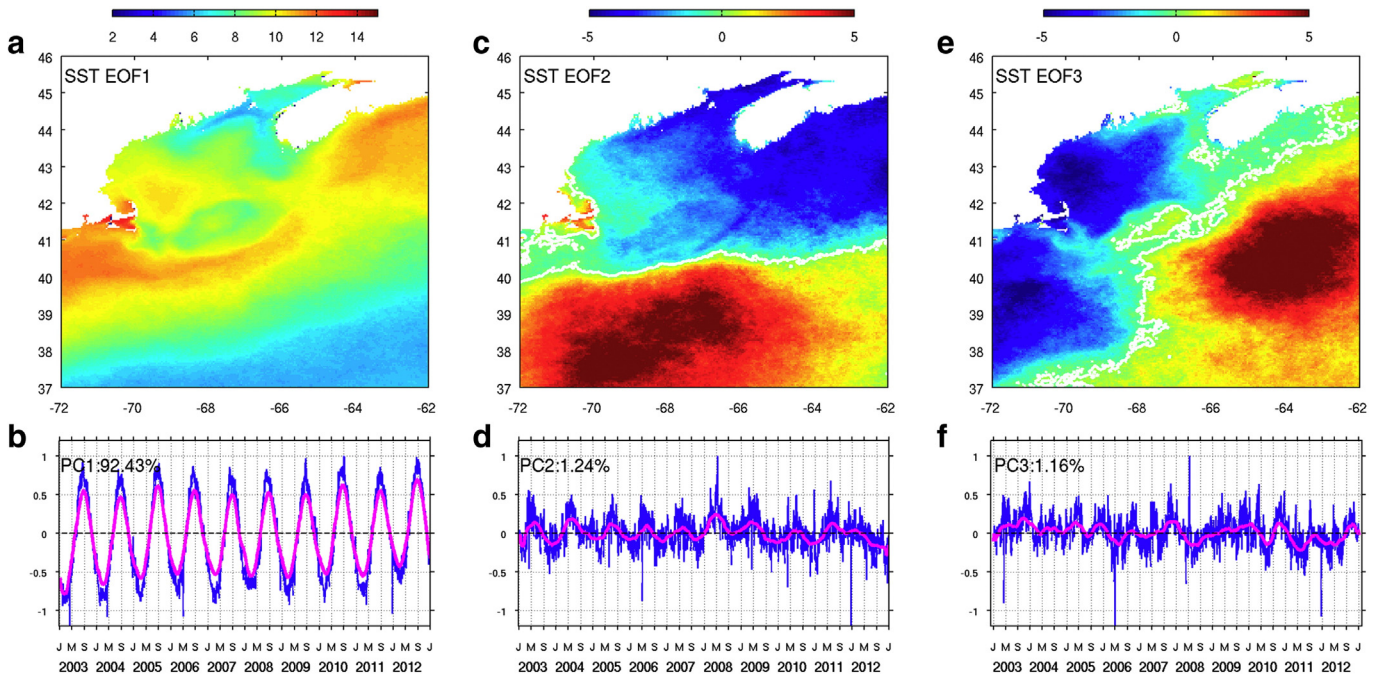
Fig. 7. Eigenfunctions (EOFs, °C, upper panels) and temporal evolution functions (PCs, lower panels) for the first three SST modes. White lines for EOF2 and EOF3 stand for the zero contour line. For each temporal evolution function, 60-day running mean (pink) is plotted on top of daily analysis (gray). The percentage of SST variance accounted for by each mode is also labeled.

The third EOF mode (accounting for 1.16% of total variance) presents a feature with a more east–west orientation. It shows an inverse variability between waters in continental slope where Labrador Slope Water converges, forming a front between the slope area and waters in the SS and Georges Bank. The cores of positive and negative anomalies are centered in the coastal western GOM and continental slope south of SS respectively. The time evolution function (PC3) shows more interannual variations instead of seasonal cycles. There also appears to be a decrease in SST in the continental slope in 2008 and 2011, when PC2 shows an increase in SST near the slope sea further south. This suggests that the variations in the Scotian-shelf/slope and

warm slope open ocean further south may be decoupled during these years. The interaction between WSW and LSW has previously been argued to perplex the hydrodynamics near Georges Bank and Northeast Channel (Smith, Houghton, Fairbanks, & Mountain, 2001).

4.2.2. Chl-a variability

We applied a natural logarithmic scale to the Chl-a field prior to the EOF decomposition. Therefore the values shown in the EOFs are in log scale relative to the mean field (Fig. 8d).

The first EOF mode (accounting for 42.74% of total variance) is dominated by the seasonal bloom peaking in spring and fall over the GOM
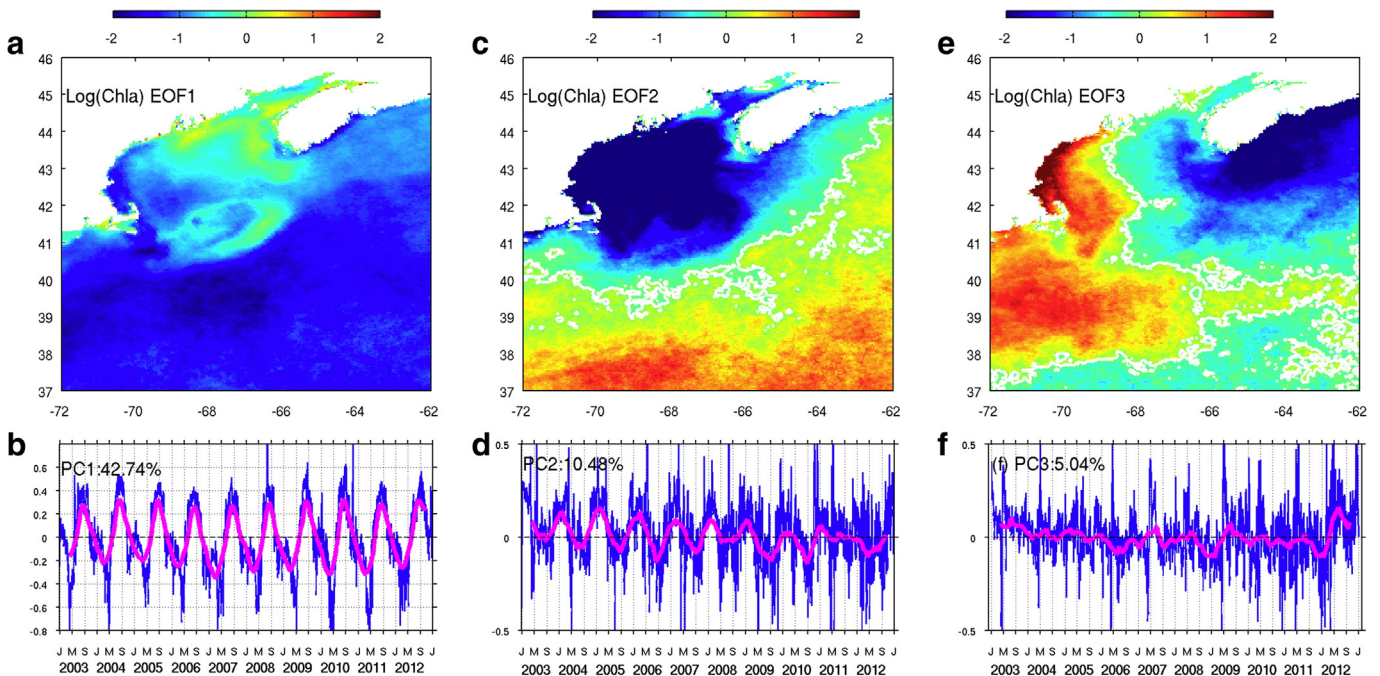

Fig. 8. Same as Fig. 7, but for Chl-a. A natural logarithmic scale was applied to the Chl-a field before the EOF analysis.

and the broader upstream region near the Scotian Shelf. The seasonal cycle associated with this EOF mode is larger in the eastern GOM and Georges Bank. There stronger tidal mixing stirs up the water column and bring the deeper nutrient upward, which in turn favors the phytoplankton bloom. The spatial EOF separates the tidal-dominated shallow water regime with deep ocean basins in the GOM. In addition, the bloom south of the Great South Channel is out of phase with the seasonal cycle inside the GOM, a feature already demonstrated in Section 3.2. As such, mode 1 is a good representation of difference in the timing of the bloom. The out-of-phase seasonality between waters in the GOM and the Slope Sea is consistent with previous studies. For example, Eslinger, O'Brien, and Iverson (1989) showed out-of-phase variability of bloom south of Georges Bank with GOM interior in 1979. Yoder et al. (2001) also found poor correlation in temporal evolution of Chl-a between GB and shelf region further south.

The second EOF mode (accounting for 10.48% of total variance) shows a seasonal cycle different from the first mode. It shows inverse relationship between shallow water over the entire Continental Shelf and slope sea further south. The time evolution function peaks in each winter and summer, maximizing in November–January and minimizing in June–August for the Continental Slope. There is also a secondary bloom in fall. Thus, mode 2 highlights evolutions of the deep-ocean bloom which is out-of-phase with the bloom in the GOM and upstream region, consistent with findings of Thomas et al. (2003) and Yoder et al. (2002). In addition, we postulate that this mode is likely associated with nutrient supply from the deep and warm slope sea. The subsurface slope water is nutrient rich, and thus offers important supplies from the subsurface (e.g., Townsend, Rebuck, Thomas, Karp-Boss, & Gettings, 2010). The winter bloom in the warm slope of MAB consumes nutrient in the south, and hence restrict the bloom in the gulf interior.

Mode 3 (accounting for 5.04% of total variance) indicates a possible influence of boundary inflow from the Scotian Shelf. The temporal evolution is highly oscillatory. The spatial EOF suggests an out-of-phase relationship between blooms in the western GOM and eastern GOM and MAB. The advection of SSW delivers nutrient-poor surface water to the eastern GOM and Jordan Basin. In addition, the progression of fresh surface SSW brings nutrient-poor water condition further

downstream, but has limited effect for the western GOM. As a result, the SSW inflow may have dampened the Chl-a bloom in the western GOM, whereas water conditions continue to favor the bloom in the western GOM and New England shelf. Thus, the third mode is likely to be related to the stability induced by ocean advection of low-salinity water from the SS. Our finding is consistent with Ji et al. (2007) showing the significance of salinity in the SS in modulating the phytoplankton bloom, and that the freshening in the eastern GOM has limited effect on the bloom condition in the western GOM. Overall, the first three modes explain 59% of the total Chl-a variance. To analyze the remaining 41% of the variability would require the analysis of high order modes.

4.2.3. Response of low-frequency SST/Chl-a variability to basin scale forcing

The low-frequency segments of SST and Chl-a signals have complex variability in response to various atmospheric forcing at different timescales. Here we focus on the SST variability in response to changes of basin-scale atmospheric forcing.

As discussed above, the first EOF mode of SST is dominated by a seasonal cycle. To compare with the surface forcing, we computed the surface net heat flux using NCEP reanalysis averaged over the research domain (Fig. 9a). The normalized net heat flux shows a similar peak as PC1, but leading the SST phase by 1–2 months. Lag correlation analysis confirms that SST signal lags the surface heat flux by 1.9 months (57-days). The lag of SST cycle over the air–sea heat flux cycle, usually called the "oceanic heat storage phase lag" (g), has been documented in the past. Li, Bye, Gallagher, and Cowan (2012) showed that with ocean advection neglected, the lag time can be estimated based on a one-dimensional model. For 40°N, the lag time is estimated to be 1.7 months, which is overall consistent with our result here. In addition to mode 1, the out-of-phase spatial relationship in both mode 2 and mode 3 suggested the interaction between coastal waters in the GOM and the Slope Sea, which is consistent earlier in the finding of Yoder et al.(2002) based on CZCS SST climatology. It has been found in previous studies (Drinkwater, Mountain, & Herman, 1999; Pershing et al., 2001; Thomas et al., 2003) that the water properties near the Northeast Channel associated with slope water oscillations may be related to large scale forcing signals such as the North Atlantic Oscillations (NAO). For
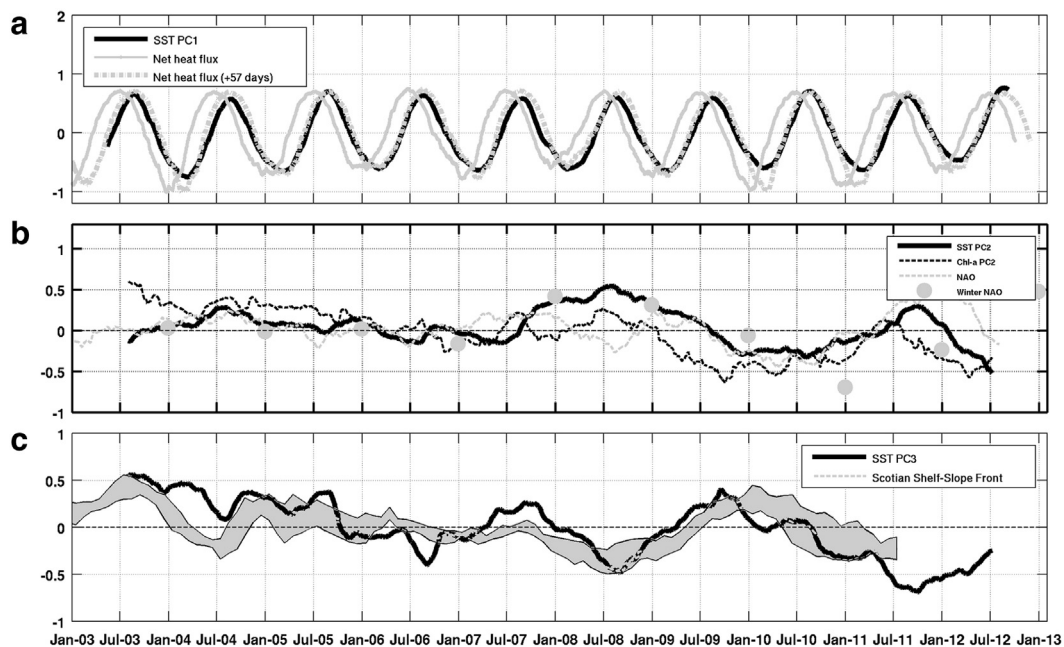

Fig. 9. (a) SST PC1 (black solid line) overlaid with normalized NCEP net heat flux time series (gray solid line) and its 57-day lagged rendition (gray dashed line). (b) SST PC2 (black solid line) and Chl-a PC2 (black dashed line) overlaid with daily NAO index (gray dashed line) and annual winter NAO index (gray dots). (c) SST PC3 (black) overlaid with normalized Scotian Shelf-slope frontal locations between 60 and 63°W(gray shaded lines). In order to better represent interannual variability, time series in (b) and (c) all underwent a 150-day running mean to remove synoptic and intra-seasonal variations, following Venegas et al. (2008).

example, Thomas et al. (2003) analyzed the satellite SST during 1997–2001 and relate the colder SST in 1998 to a positive NAO index. They argued that during positive NAO phase, less WSW from the south are entrained into the GOM, and subsequently led a regional SST drop in 1998.

Based on our longer time series in this study, we compared the PC2 time series with both low-frequency NAO index and winter NAO index. To retain only the low-frequency variability, both SST and Chl-a PC2 and daily NAO indices are 150-day running-averaged, following the approach used in Venegas et al. (2008). We found that the SST and Chl-a PC2 are overall in phase. There is also a good correlation between the PC2s and NAO index (Fig. 9b). Over the 10-year study period, the SST PC2s is largely in-phase with NAO variability. The only exception is in 2008, when a low NAO index seems to coincide with high SST/Chl-a PC indices. However, the winter NAO index is largely negative in 2008 and 2009, suggesting that winter NAO index may provide more impact on the SST/Chl-a variability during this period.

To analyze the possible mechanism accounting for the SST mode 3, we compared the time series (shown in blue line) with the Scotian Shelf-slope front location index produced by Bedford Institute of Oceanography, Canada (Fig. 9c). The strong coherence between the two signals suggests that mode 3 is likely dominated by the cross-shelf (east–west) displacement of the Shelf-Slope front near 60–63°W. We also noticed that the spatial variations in SST mode 3 are out of phase between GOM and slope sea. A possible candidate mechanism is that when there is a subsurface intrusion of slope water into the gulf, SST in the continental slope decreases due to the overall heat loss from advection. In the meantime, there can be an increase in the SST inside the gulf as a result of heat supply from the subsurface warm water intrusion. It also shows that EOF can be used as an alternative tool to identify the overall location of the SSW front.

In addition to SST, we also investigated the relationship between SST and Chl-a and the linkage between the variability of Chl-a and large-scale forcing. No clear relationship was found between SST and Chl-a on interannual timescale for other major EOF modes except for mode 2. The coincidence between SST and Ch-a variability in mode 2 suggests that the two variables are coupled during most years. Thomas et al. (2003) postulated that the coupling between SST and Chl-a as shown in PC2 is likely due to decreased inflow of nutrient-rich warm slope waters from subsurface, which favors a weaker Chl-a bloom, as well as decreased SST through vertical mixing. This was further evidenced by the regime-shift of nutrient condition suggested by Townsend et al. (2010). Despite the coherence of PC2 in SST and Chl-a in 2009, 2010, and 2012, the two variables seem decoupled in other years such as 2003, when negative SST anomaly in the GOM is coincident with positive Chl-a concentration. The direct relationship between Chl-a and NAO is not as clear as that for SST PC2, suggesting that other mechanisms are responsible for the Chl-a interannual variability. The offshore nutrient flux, wind forcing, coastal riverine nutrient discharge, water stratification, and upper trophic biomass are all possible factors accounting for Chl-a variations.

5. Summary and conclusion

The spatial and temporal variability of the SST and Chl-a was examined using a decade long cloud-free DINEOF SST and Chl-a analysis. The SST showed a sinusoidal seasonal cycle. Positive SST anomalies were present in 2005, 2010 and 2012 in response to the variations in surface heat flux. The first SST EOF mode was dominated by an annual periodicity peaking in summer and winter, and the signal lags the surface net heat flux by ~50 days. Further analysis showed that the magnitude of the seasonal cycle at different locations in the GOM is a result of water depth, tidal rectification and heat flux redistribution. The second EOF mode started to include some synoptic time-scale oscillations, an annual cycle, as well as interannual variability. The PC2 reached its peak in May–July and its minimum in December to February. A dipole-like feature with north–south orientation was present in the second spatial EOF, which suggests an out-of-phase variability between waters in Slope Sea and in the GOM. It underscored the interactions between broad GOM and the slope sea region in response to large scale forcing variability (such as the North Atlantic Oscillation). The third mode showed more interannual variations instead of seasonal cycles, which is likely responding to the Scotian Shelf-Slope frontal dynamics.

Chl-a variability was generally dominated by a spring bloom with a secondary fall bloom in the GOM. The different timing in the spring and fall blooms was identified. There is an overall increasing trend in surface Chl-a bloom during 2003–2011, and decreasing thereafter. The first EOF mode showed stronger seasonal variability in the area with stronger tidal forcing. The second mode presented an out-of-phased relationship in the waters between GOM and the open ocean slope sea, and is highly in phase with the second mode of SST. Therefore, mode 1 and mode 2 represented responses of Chl-a bloom to both local and atmospheric forcing, both of which may have significant impact on higher trophic cascade such as shrimp hatching processes (Koeller et al., 2009). Moreover, the highly in-phase variation between SST and Chl-a PC2s and NAO index suggests a possible linkage between atmospheric forcing and coupled ocean physical–biological interaction. Mode 3 was likely associated with the effect of fresh water advected from the upstream on the bloom in the coastal GOM. In addition to the delivery of nutrient-poor ocean condition to the eastern GOM, the fresh SSW helps to establish stratification that impedes the nutrient uptake in the eastern GOM. The salinity impact, however, has limited effect on the western GOM and phytoplankton bloom further downstream (Ji et al., 2007) in the western GOM.

The DINEOF analysis herein provides a useful dataset for investigating the spatial and temporal variability of the coastal SST and Chl-a. We note however that satellite remote sensing observes only the near surface layer of the ocean. Their data are short by climate standards (Antoine, Morel, Gordon, Banzon, & Evans, 2005) because they cannot address physical and biological properties over the entire water column (Platt & Herman, 1983). The chlorophyll can have a peak at subsurface, representing a phytoplankton biomass maximum that occurs at a depth where both light and nitrate availability allow net growth of the population (Holligan et al., 1984). High concentration of surface pigment could come from either 1) biomass enhancement stimulated by the introduction of nutrient into surface euphotic layer, or 2) vertical advection of colored materials from their subsurface maxima (He et al., 2010; McGillicuddy, Kosnyrev, Ryan, & Yoder, 2001). The trend of Chl-a variation in the recent year is likely associated with the nutrient regime shift in the GOM (Townsend et al., 2010). Finally, the satellite-derived coastal ocean color is subject to contamination by CDOM and suspended sediment, the composite of which is largely unknown. As such, more subsurface Chl-a and nutrient information are needed to better understand the dynamic of phytoplankton blooms and their linkage with climate signals.

References

Alvera-Azcárate, A., Barth, A., Beckers, J. -M., & Weisberg, R. H. (2007). Multivariate reconstruction of missing data in sea surface temperature, chlorophyll and wind satellite fields. *Journal of Geophysical Research*, *112*, C03008. http://dx.doi.org/10.1029/2006JC003660.

Alvera-Azcárate, A., Barth, A., Rixen, M., & Beckers, J. -M. (2005). Reconstruction of incomplete oceanographic data sets using Empirical Orthogonal Functions. Application to the Adriatic Sea. *Ocean Modelling*, *9*, 325–346.

Alvera-Azcárate, A., Barth, A., Sirjacobs, D., & Beckers, J. -M. (2009). Enhancing temporal correlations in EOF expansions for the reconstruction of missing data using DINEOF. *Ocean Science*, *5*, 475–485.

Antoine, D., Morel, A., Gordon, H. R., Banzon, V. F., & Evans, E. H. (2005). Bridging ocean color observations of the 1980s and 2000s in search of long-term trends. *Journal of Geophysical Research*, *110*. http://dx.doi.org/10.1029/2004JC002620.

Beckers, J. -M., Barth, A., & Alvera-Azcarate, A. (2006). DINEOF reconstruction of clouded images including error maps. Application to the Sea Surface Temperature around Corsican Island. *Ocean Science*, *2*(2), 183–199.

Bigelow, H. B. (1927). Physical oceanography of the Gulf of Maine. *Fisheries Bulletin*, *40*, 511–1027.

Bisagni, J. J., & Smith, P. C. (1998). Eddy-induced flow of Scotian Shelf water across Northeast Channel, Gulf of Maine. *Continental Shelf Research*, *18*, 515–539.

Chaudhuri, A., Gangopadhyay, A., & Bisagni, J. J. (2009). Interannual variability of Gulf Stream warm-core rings in response to the North Atlantic Oscillation. *Continental Shelf Research*, *29*(7), 856–869 (15 April 2009).

Churchill, J. H., Pettigrew, N. R., & Signell, R. P. (2005). Structure and variability of the Western Maine Coastal Current. *Deep Sea Research, Part II*, *52*(19–21), 2392–2410.

Drinkwater, K. F., Mountain, D. B., & Herman, A. (1999). Variability in the slope water properties off eastern North America and their effects on the adjacent shelves. *ICES CM*, *8*, 26.

Eslinger, D. L., O'Brien, J. J., & Iverson, R. L. (1989). EOF analysis of cloud contaminated coastal zone color scanner images of northeastern North American coastal waters. *Journal of Geophysical Research*, *94*, 10884–10890.

Garrett, C. (1972). Tidal resonance in the Bay of Fundy and Gulf of Maine. *Nature*, *238*, 441–443.

He, R., Chen, K., Moore, T., & Li, M. (2010). Mesoscale variations of sea surface temperature and ocean color patterns at the Mid-Atlantic Bight shelfbreak. *Geophysical Research Letters*. http://dx.doi.org/10.1029/2010GL043067.

He, R., & McGillicuddy, D. J. (2008). Gulf of Maine circulation and harmful algal bloom in Summer 2005 — Part 1: In-situ observation. *Journal of Geophysical Research*, *113*, C07039. http://dx.doi.org/10.1029/2007JC004691.

He, R., McGillicuddy, D. J., Smith, K. W., Lynch, D. R., Stock, C. A., & Manning, J. P. (2005). Data assimilative hindcast for the Gulf of Maine coastal circulation. *Journal of Geophysical Research*, *110*. http://dx.doi.org/10.1029/2004JC002807 (C10, C10011).

He, R., & Weisberg, R. H. (2003). West Florida shelf circulation and temperature budget for 1998 fall transition. *Continental Shelf Research*, *23*(8), 777–800.

He, R., Weisberg, R. H., Zhang, H., Muller-Karger, F. E., & Helber, R. W. (2003). A cloud free satellite-derived, sea surface temperature analysis for the West Florida Shelf. *Geophysical Research Letters*, *30*(15), 1811. http://dx.doi.org/10.1029/2003GL017673.

Herman, A. W., Sameoto, D.D., Shunnian, C., Mitchell, M. R., Petrie, B., & Cochrane, N. (1991). Sources of zooplankton on the Nova Scotia shelf and their aggregations within deep shelf basins. *Continental Shelf Research*, *11*, 211–238.

Holligan, P.M., Balch, W. M., & Yentsch, C. M. (1984). The significance of subsurface chlorophyll, nitrite and ammonium maxima in relation to nitrogen for phytoplankton growth in stratified waters of the Gulf of Maine. *Journal of Marine Research*, *42*, 1051–1073.

Ji, R., Davis, C., Chen, C., Townsend, D., Mountain, D., & Beardsley, R. (2007). Influence of ocean freshening on shelf phytoplankton dynamics. *Geophysical Research Letters*, *34*, L24607. http://dx.doi.org/10.1029/2007GL032010.

Koeller, P., et al. (2009). Basin-scale coherence in phenology of shrimps and phytoplankton in the North Atlantic Ocean. *Science*, *324*(5928), 791–793.

Li, C. -L., Bye, J. A. T., Gallagher, S. J., & Cowan, T. (2012). Annual sea surface temperature lag as an indicator of regional climate variability. *International Journal of Climatology*. http://dx.doi.org/10.1002/joc.3587.

Li, Y., He, R., & McGillicuddy, D. J. (2013). Seasonal and interannual variability in Gulf of Maine hydrodynamics: 2002–2011. *Deep-Sea Research II*, in press (http://dx.doi.org/10.1016/j.dsr2.2013.03.001).

Limeburner, R., & Beardsley, R. C. (1996). Near-surface recirculation over Georges Bank. *Deep Sea Research II*, *43*, 1547–1574.

Luerssen, R. M., Thomas, A.C., & Hurst, J. (2005). Relationships between satellite-measured thermal features and Alexandrium-imposed toxicity in the Gulf of Maine. *Deep Sea Research, Part II*, *52*, 2656–2673.

Lynch, D. R., Holboke, M. J., & Maimie, C. E. (1997). The Maine coastal current: Spring climatological circulation. *Continental Shelf Research*, *17*, 605–639.

Lynch, D. R., Ip, J. T. C., Naimie, C. E., & Werner, F. E. (1996). Comprehensive coastal circulation model with application to the Gulf of Maine. *Continental Shelf Research*, *16*(7), 875–906.

McGillicuddy, D. J., Kosnyrev, V. K., Ryan, J. P., & Yoder, J. A. (2001). Covariation of mesoscale ocean color and sea surface temperature patterns in the Sargasso Sea. *Deep-Sea Research II*, *48*, 1823–1836.

McGillicuddy, D. J., Townsend, D. W., He, R., Keafer, B.A., Kleindinst, J. L., Li, Y., et al. (2011). Suppression of the 2010 Alexandrium fundyense bloom by changes in physical, biological, and chemical properties of the Gulf of Maine. *Limnology and Oceanography*, *56*(6), 2411–2426.

Miles, T., & He, R. (2010). Seasonal surface ocean temporal and spatial variability of the South Atlantic Bight: Revisiting with MODIS SST and Chl-a imagery. *Continental Shelf Research*. http://dx.doi.org/10.1016/j.csr.2010.08.016.

Miles, T. N., He, R., & Li, M. (2009). Characterizing the South Atlantic Bight seasonal variability and cold water event in 2003 using a daily cloud-free SST and chlorophyll analysis. *Geophysical Research Letters*, *36*, L02604. http://dx.doi.org/10.1029/2008GL036393.

O'Reilly, J. E., Evans-Zetlin, C., & Busch, D. A. (1987). Primary production. In R. H. Backus (Ed.), *Georges Bank* (pp. 221–233). Cambridge, MA: MIT Press.

O'Reilly, J. E., & Busch, D. A. (1984). Phytoplankton primary production on the northwestern Atlantic shelf. *Rapports et procès-verbaux desréunions*, *183*, 255.

Pershing, A. J., Greene, C. H., Hannah, C., Sameoto, D., Head, E., Mountain, D., et al. (2001). Oceanographic responses to climate in the Northwest Atlantic. *Oceanography*, *14*, 76–82.

Pettigrew, N. R., Churchill, J. H., Janzen, C. D., Mangum, L. J., Signell, R. P., Thomas, A.C., et al. (2005). The kinematic and hydrographic structure of the Gulf of Maine coastal current. *Deep Sea Research, Part II*, *52*(19–21), 2369–2391.

Pettigrew, N. R., Townsend, D. W., Xue, H., Wallinga, J. P., Brickey, P. J., & Hetland, R. D. (1998). Observations of the Eastern Maine Coastal Current and its offshore extensions. *Journal of Geophysical Research*, *103*(30), 623–640.

Platt, T., & Herman, A. W. (1983). Remote sensing of phytoplankton in the sea: Surface-layer chlorophyll as an estimate of water column chlorophyll and primary production. *International Journal of Remote Sensing*, *4*(2), 343–351.

Rebuck, N. D. (2011). *Nutrient distributions in the Gulf of Maine: An analysis of spatial and temporal patterns of dissolved inorganic nitrate and silicate.* PhD Dissertation. Orono: University of Maine.

Ryan, J. P., Yoder, J. A., & Cornillon, P. C. (1999). Enhanced chlorophyll at the shelfbreak of the mid-Atlantic Bight and Georges Bank during the spring transition. *Limnology and Oceanography*, *44*, 1–11.

Sirjacobs, D., Alvera-Azcárate, A., Barth, A., Lacroix, G., Park, Y., Nechad, B., et al. (2011). Cloud filling of ocean colour and sea surface temperature remote sensing products over the Southern North Sea by the Data Interpolating Empirical Orthogonal Functions methodology. *Journal of Sea Research*, *65*(1), 114–130. http://dx.doi.org/10.1016/j.seares.2010.08.002.

Smith, P. C. (1983). The mean and seasonal circulation off southeast Nova Scotia. *Journal of Physical Oceanography*, *13*, 1034–1054.

Smith, P. C., Houghton, R. W., Fairbanks, R. G., & Mountain, D.G. (2001). Interannual variability of boundary fluxes and water mass properties in the Gulf of Maine and on Georges Bank: 1993–1997. *Deep-Sea Research II*, *48*, 37–70.

Thomas, A.C., Townsend, D. W., & Weatherbee, R. (2003). Satellite-measured phytoplankton variability in the Gulf of Maine. *Continental Shelf Research*, *23*, 971–989. http://dx.doi.org/10.1016/S0278-4343(03)00086-4.

Thomas, A.C., Weatherbee, R., Xue, H., & Liu, G. (2010). Interannual variability of shellfish toxicity in the Gulf of Maine: Time and space patterns and links to environmental variability. *Harmful Algae*, *9*, 458–480. http://dx.doi.org/10.1016/j.hal.2010.03.002.

Townsend, D. W., Cammen, L. M., Holligan, P.M., Campbell, D. E., & Pettigrew, N. R. (1994). Causes and consequences of variability in the timing of spring phytoplankton blooms. *Deep-Sea Research I*, *41*, 747–765.

Townsend, D. W., Rebuck, N. D., Thomas, M.A., Karp-Boss, L., & Gettings, R. M. (2010). A changing nutrient regime in the Gulf of Maine. *Continental Shelf Research*, *30*, 820–832.

Townsend, D. W., & Thomas, A.C. (2001). Winter–Spring Transition of phytoplankton chlorophyll and inorganic nutrients on Georges Bank. *Deep-Sea Research II*, *48*, 199–214.

Townsend, D. W., & Thomas, M. (2002). Springtime nutrient and phytoplankton dynamics on Georges Bank. *Marine Ecology — Progress Series*, *228*, 57–74.

Trees, Charles C., Kennicutt, Mahlon C., II, & Brooks, James M. (1985). Errors associated with the standard fluorimetric determination of chlorophylls and phaeopigments. *Marine Chemistry*, *17*(1), 1–12.

Ullman, D. S., & Cornillon, P. C. (1999). Satellite-derived sea surface temperature fronts on the continental shelf off the northeast US coast. *Journal of Geophysical Research: Oceans (1978–2012)*, *104*(C10), 23459–23478.

Venegas, R. M., Strub, P. T., Beier, E., Letelier, R., Thomas, A.C., Cowles, T., et al. (2008). Satellite-derived variability in chlorophyll, wind stress, sea surface height, and temperature in the northern California Current System. *Journal of Geophysical Research*, *113*, C03015. http://dx.doi.org/10.1029/2007JC004481.

Volpe, G., Buongiorno Nardelli, B., Cipollini, P., Santoleri, R., & Robinson, I. S. (2012). Seasonal to interannual phytoplankton response to physical processes in the Mediterranean Sea from satellite observations. *Remote Sensing of Environment*, *117*, 223–235. http://dx.doi.org/10.1016/j.rse.2011.09.020.

Xue, H., Chai, F., & Pettigrew, N. R. (2000). A model study of the seasonal circulation in the Gulf of Maine. *Journal of Physical Oceanography*, *30*(5), 1111–1135.

Yoder, J. A., O'Reilly, J. E., Barnard, A. H., Moore, T. S., & Ruhsam, C. M. (2001). Variability in coastal zone color scanner (CZCS) chlorophyll imagery of ocean margin waters off the US East Coast. *Continental Shelf Research*, *21*, 1191–1218.

Yoder, J. A., Schollaert, S., & O'Reilly, J. E. (2002). Climatological phytoplankton chlorophyll and sea surface temperature patterns in continental shelf and slope waters off the northeast US Coast. *Limnology and Oceanography*, *47*, 672–682.

Zhao, Y., & He, R. (2012). Characterizing the Gulf of Mexico SST and ocean color variability using a cloud-free satellite data analysis. *Remote Sensing Letters*, *3*(8), 697–706.